

Supplementary material

Supplement S1: Synthesis of corrections and choices when computing fluxes and drivers

1. Data

We used 24 years (1997–2020) of half-hourly eddy-covariance and meteorological measurements from the ICOS forest ecosystem station FR-Hes, located in a mature, beech-dominated temperate forest. During the study period, fluxes were acquired successively from three tower configurations with measurement heights of 18 m (1997–1999), 23.34 m (2000–2012), and 27.1 m (2013–2020). Footprint analyses consistently showed that at least 80 % of the measured flux originated from the beech-dominated area of the forest, ensuring temporal comparability across tower configurations.

2. Quality control filtering

We applied all quality flags generated during eddy-covariance processing to ensure that only reliable turbulent fluxes were retained. Half-hours failing either stationarity or integral turbulence characteristics tests were discarded for the affected variables, specifically: CO₂ flux (FC), and associated net ecosystem exchange (NEE) estimates, latent heat (LE), and sensible heat (H). In addition, several short periods influenced by snow cover or instrumentation issues were manually excluded based on site operator documentation.

3. Backup measurements

Missing meteorological variables were reconstructed using adaptive windowed linear regression between co-located sensors measuring the same quantity. For each missing value, a linear regression was fitted within a moving window centered on the gap, beginning with 7 days and expanding in 7-day increments up to a maximum window length. A regression was accepted only when:

- at least 5 days of valid data and at least one-third of window values were available,
- the predicted value did not require substantial extrapolation,
- the regression achieved $R^2 \geq 0.8$.

This procedure was applied to variables with redundant sensors (e.g., air temperature, humidity, radiation, precipitation).

4. CO₂ storage flux

The below-canopy CO₂ storage flux (SC) was computed from vertical CO₂ concentration profiles measured within the canopy and trunk space. For each height level i , temporal CO₂ changes were estimated as half-hour finite differences (dC_i/dt). The vertically integrated storage term was calculated as:

$$SC = \rho \sum_i \frac{dC_i}{dt} \Delta z_i$$

where Δz_i is the thickness of the layer represented by level i , derived from the midpoints between consecutive heights, and ρ is the air molar density. When the highest profile measurement was missing, the CO₂ concentration at the eddy-covariance sampling height was used as a substitute for the uppermost layer. To maximize temporal coverage, storage was additionally computed for incomplete profiles when at least four profile points were available, with layer thicknesses recalculated from the subset of available heights.

To fill remaining gaps, we used a turbulence- and season-dependent lookup table (Aubinet et al., 2018). Storage values were grouped by 0.1 m s^{-1} friction velocity (u^*) classes, month, and half-hour of day, and missing values were replaced by the corresponding class mean. Final NEE was calculated as $NEE = FC + SC$. After this procedure, 10.8 % of NEE values were missing.

5. u^* threshold estimation and filtering

Periods of insufficient turbulence were identified using a year-wise and seasonally resolved u^* approach. Two seasons were defined based on the site's climatology:

- Growing season (GS): May–September,
- Dormant season: October–April.

A two-season scheme was preferred over a four-season partition because winter periods yielded poorly constrained and spuriously high u^* thresholds.

For each year \times season combination, a bootstrap distribution of u^* thresholds was derived, and the median was retained for all subsequent analyses. NEE and H observations were restricted to periods with u^* above this threshold. LE was not u^* -filtered, as nighttime LE is typically close to zero and insensitive to u^* . Following u^* filtering, 22.9 % of NEE values were missing overall (21.5 % during GS, 23.9 % during the dormant season; 10.9 % during daytime, 35 % during nighttime).

6. MDS gapfilling of fluxes and meteorological variables

Remaining gaps in NEE, H, LE, and all meteorological drivers (air temperature, incoming solar radiation, vapor pressure deficit) were filled using the standard marginal distribution sampling (MDS) approach implemented in REddyProc. MDS relies on hierarchical selection of donor values under similar meteorological conditions, expanding the temporal window as necessary. Outlier detection was not applied to NEE, as tests with additional filters (value thresholds, second-derivative tests) showed negligible influence on final indicator values and tended to remove high-magnitude uptake events disproportionately. Nonetheless, spikes in high frequency data were already filtered upstream in the station's EC processing.

7. Partitioning

Gross primary production and ecosystem respiration were partitioned from NEE using the nighttime-based flux partitioning algorithm in REddyProc, applied independently for each year. This year-wise approach accounts for the long-term evolution of ecosystem respiration associated with forest maturation.

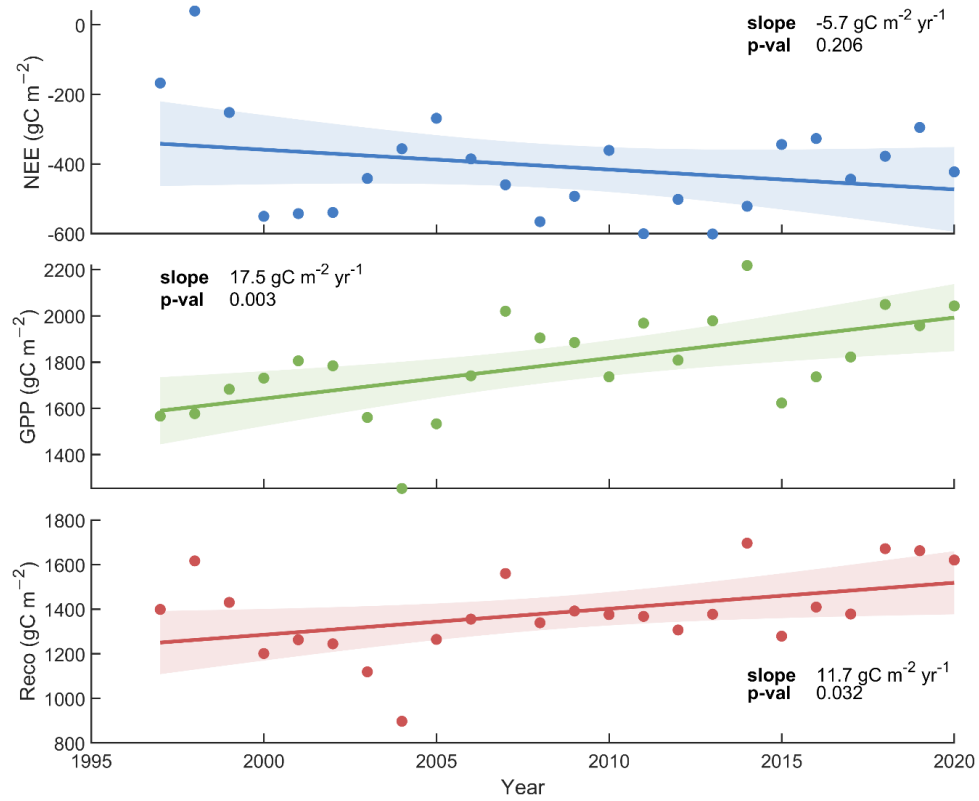


Figure S1: Interannual variability of annual net ecosystem exchange (NEE), gross primary production (GPP), and ecosystem respiration (Reco) from 1997 to 2020. Dots represent annual values and solid lines show linear trends fitted using ordinary least squares. Shaded areas indicate 95 % confidence intervals around the trend. For each flux, the estimated slope of the linear regression and its associated p-value are reported.

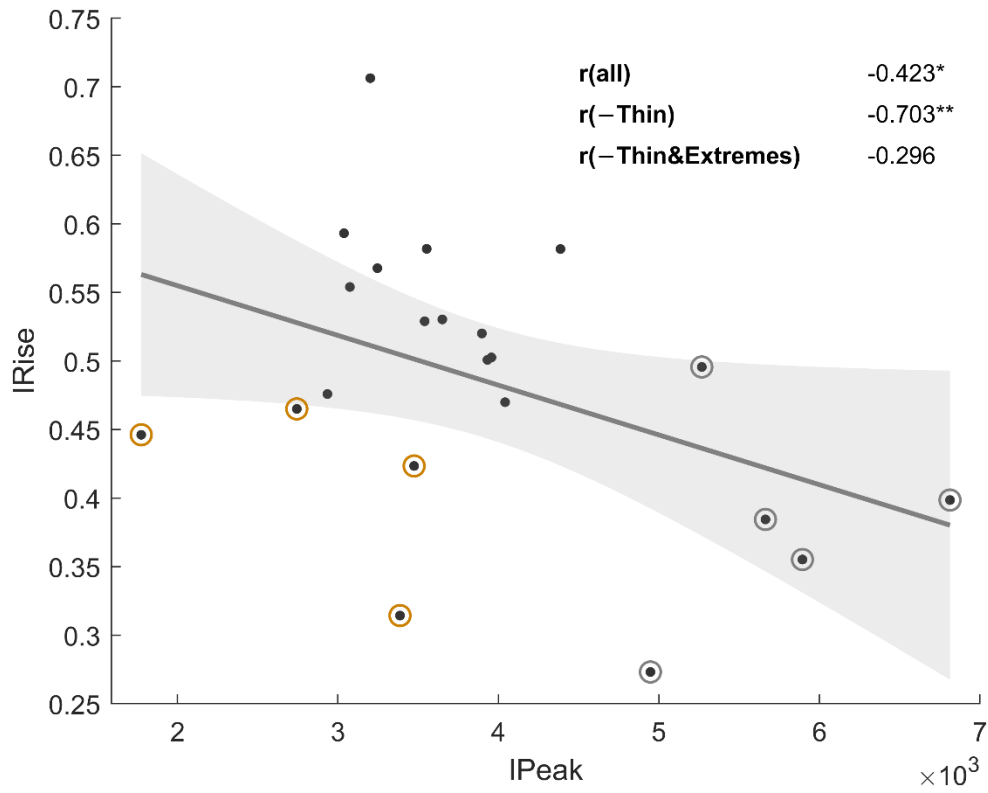


Figure S2: Scatter plot showing the relationship between IRise and IPeak. Thinning years are highlighted with yellow circles and extreme-summer years with grey circles. Correlation coefficients are reported for (1) the full time series, (2) the subset excluding thinning years, and (3) the subset excluding both thinning and extreme summer years. Statistical significance is indicated by one, two, or three stars for $p \leq 0.05$, 0.01 , and 0.001 , respectively.

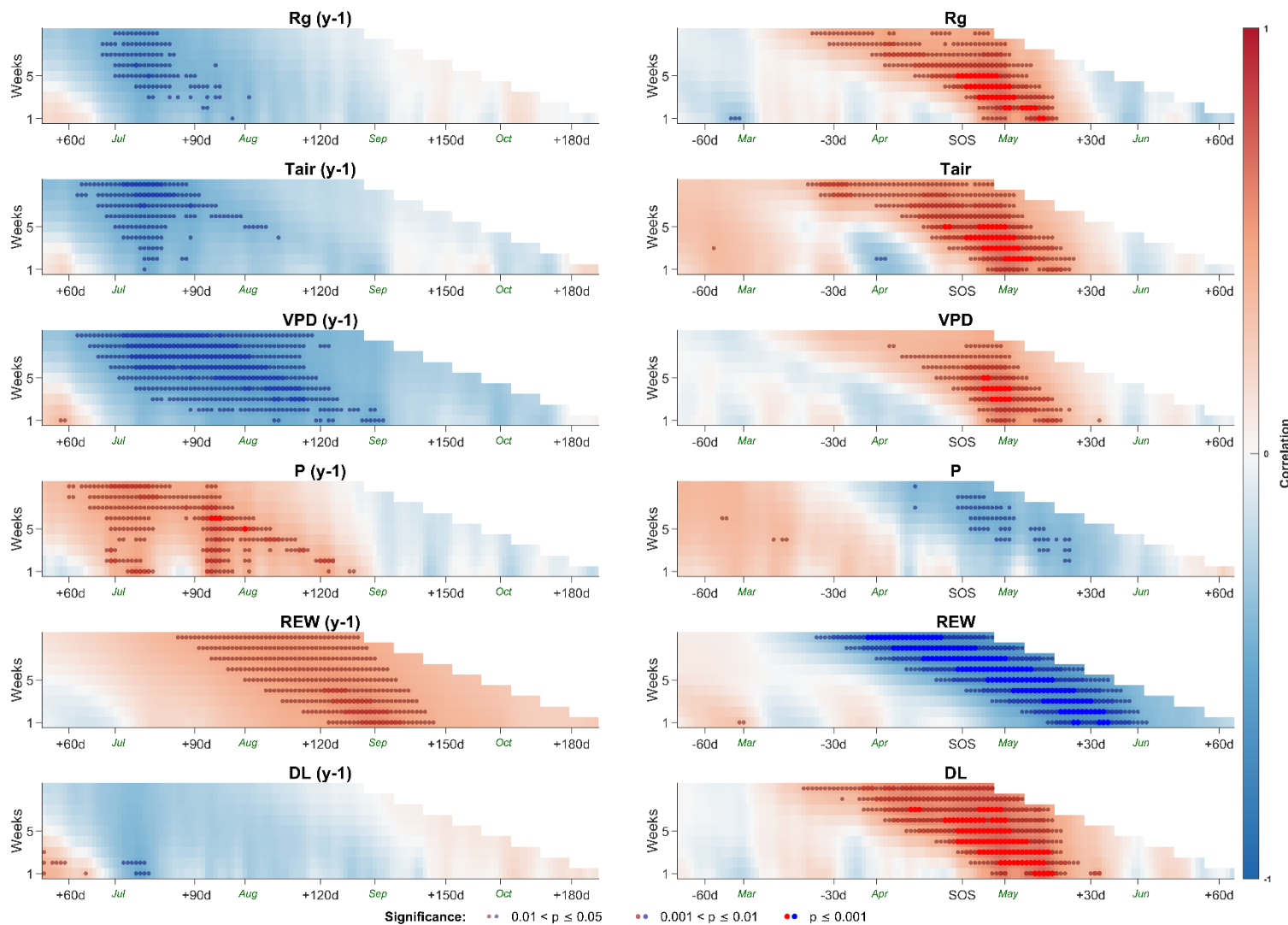


Figure S3: Correlograms depicting sliding-window Pearson correlations between IRise and environmental drivers averaged over different window sizes (y-axis, in weeks) and starting dates (x-axis, in days relative to SOS). Average calendar dates (across all years) at which each month begins are indicated in green. Correlations were computed on a 1-week \times 1-day grid and lightly smoothed using an anisotropic Gaussian filter ($\sigma_x = 0.8$ days, $\sigma_y = 1.3$ days) for clarity. Statistical significance, computed on the unsmoothed correlations, is represented by markers whose size, opacity, and color saturation scale with p-value. Colors indicate correlation sign and magnitude (red = positive; blue = negative). Left panels represent previous-year effects and right panels current-year effects.

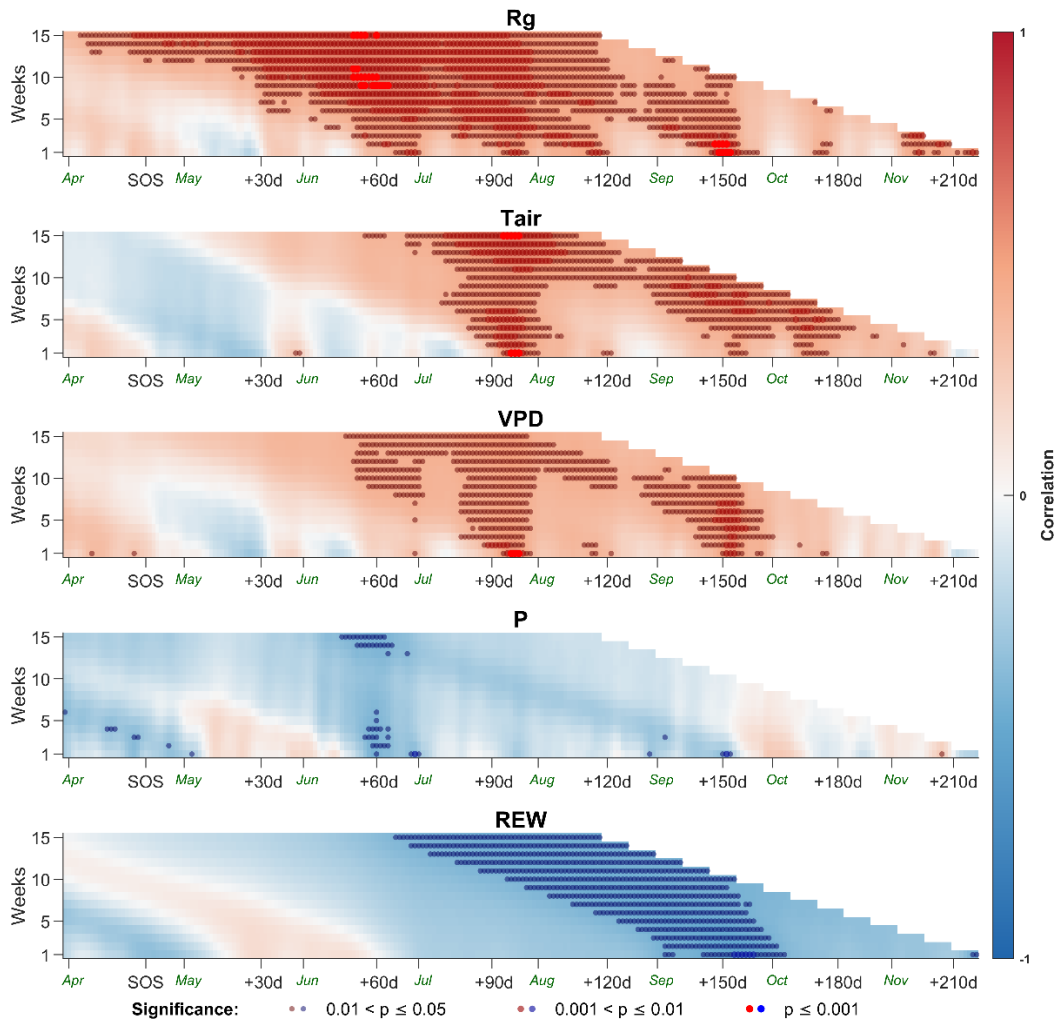


Figure S4: Correlogram depicting sliding-window Pearson correlations between IPeak and current-year environmental drivers. For methodological details and full description of correlogram structure, see Fig. S3.

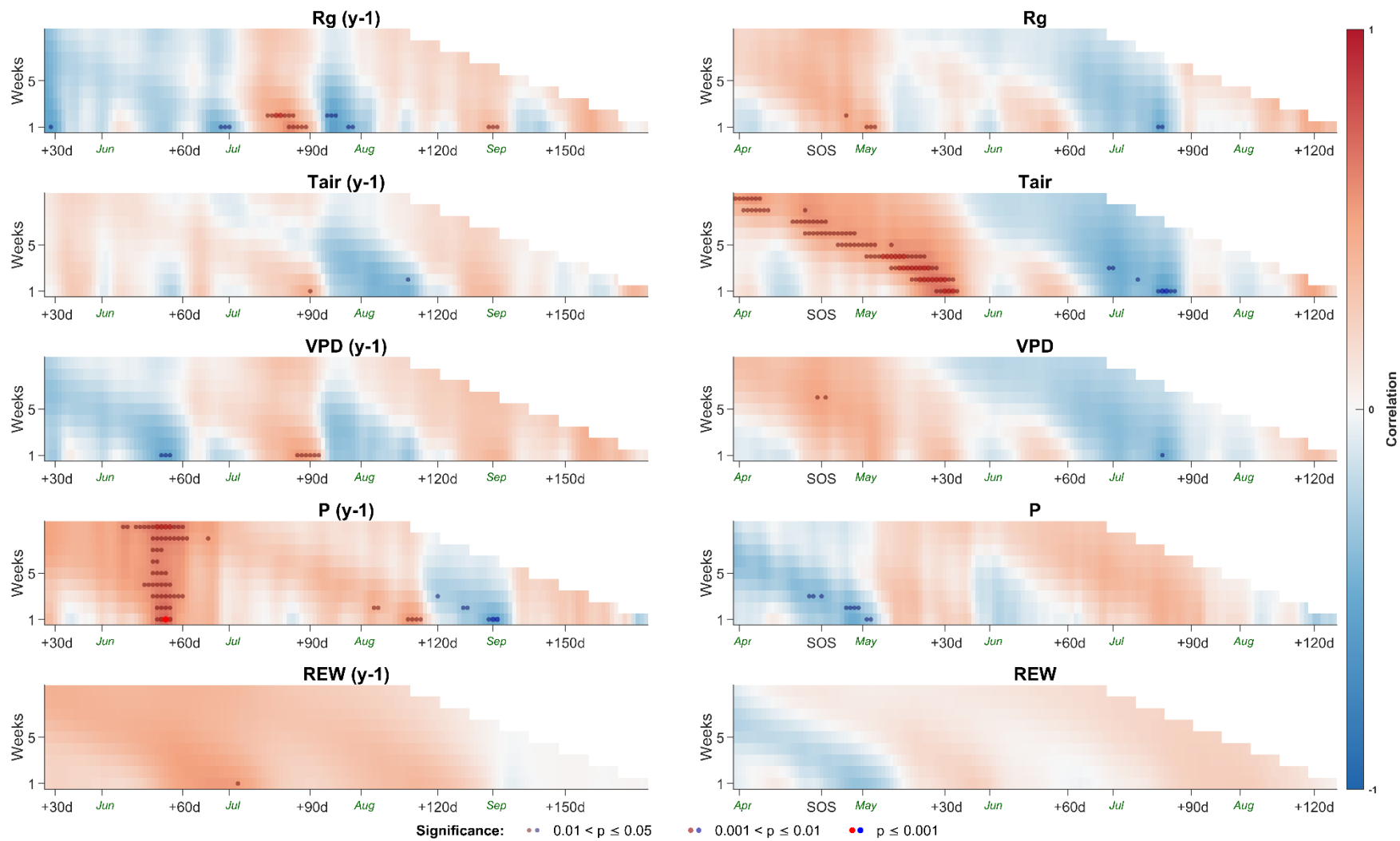


Figure S5: Correlogram depicting sliding-window Pearson correlations between IPeak and environmental drivers, excluding thinning (1999, 2005, 2010, 2016) and extreme summer (2013, 2014, 2018, 2019, 2020) years. For methodological details and full description of correlogram structure, see Fig. S3.

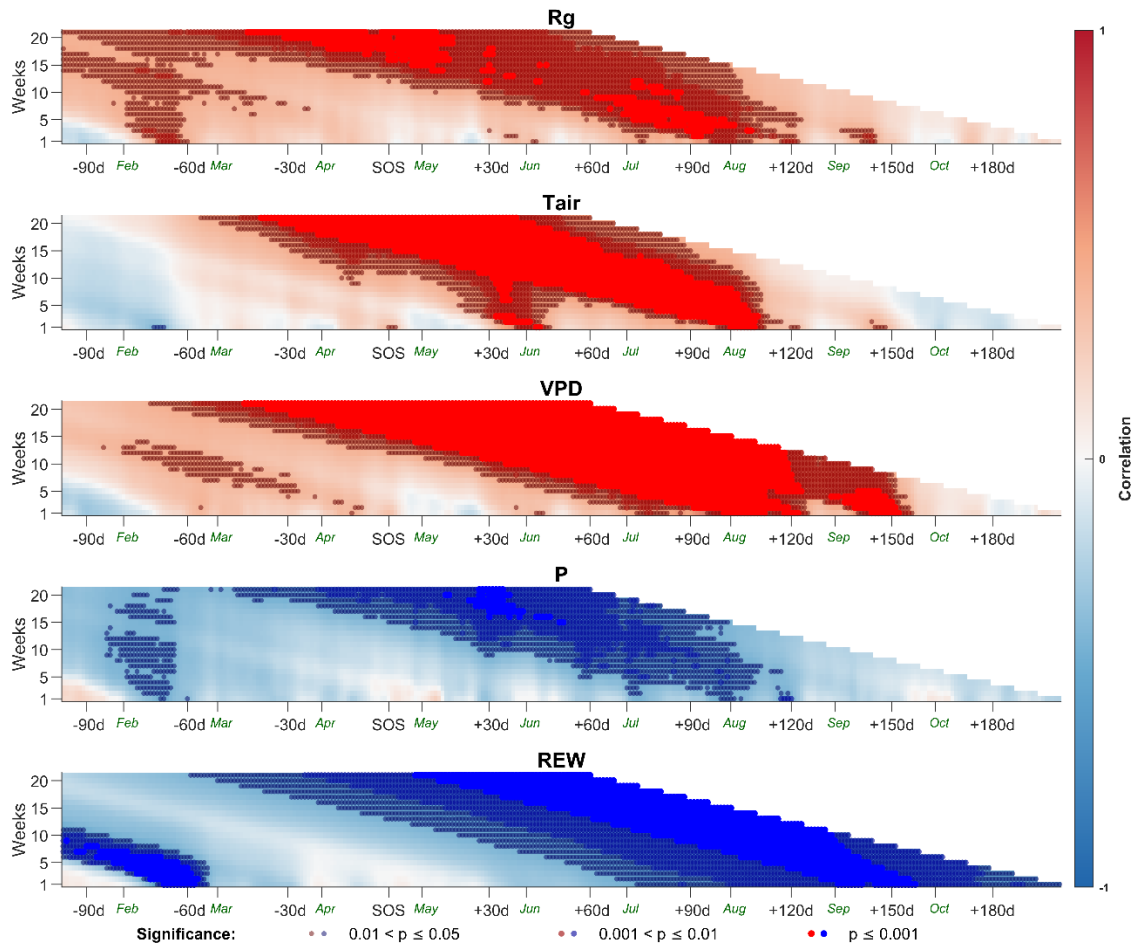


Figure S6: Correlogram depicting sliding-window Pearson correlations between IDrop and current-year environmental drivers. For methodological details and full description of correlogram structure, see Fig. S3.

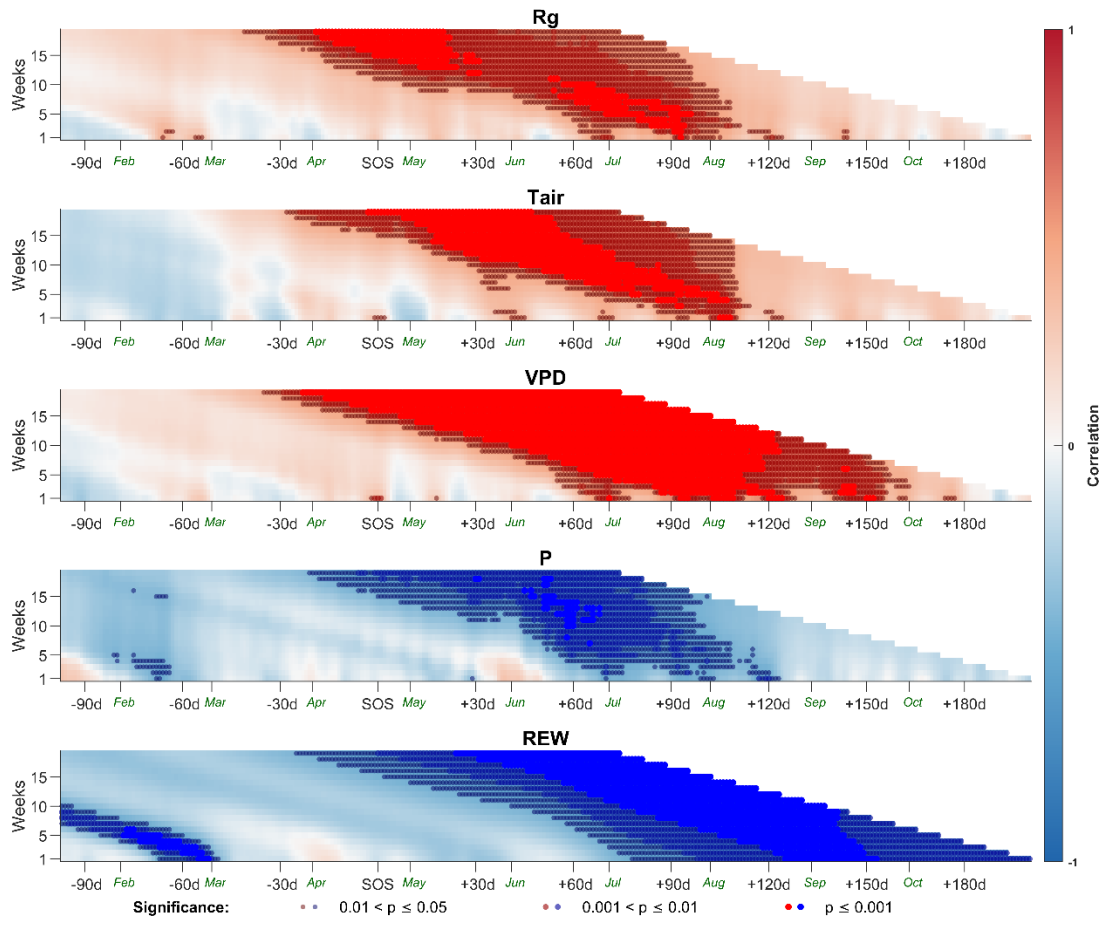


Figure S7: Correlogram depicting sliding-window Pearson correlations between IDrop and current-year environmental drivers, excluding the exceptional 2003 drought year. For methodological details and full description of correlogram structure, see Fig. S3.

Table S1: Significant correlations extracted from the IRise correlogram (Fig. S3), grouped according to previous-year and current-year influences. Variables selected through partial correlation analysis are shown in bold. Window start and end dates are expressed in days relative to SOS. Correlation coefficients are listed in the rightmost column of each section, with statistical significance indicated by one, two, or three stars for $p \leq 0.05$, 0.01 and 0.001 , respectively. The first section summarizes long-scale correlations, followed by shorter-scale correlation windows organized according to their temporal proximity.

<i>Previous year</i>					<i>Current year</i>				
	Variable	Start	End	Correlation		Variable	Start	End	Correlation
Long-scale	P_{y-1}	+95	+137	0.693***	Long-scale	Rg	+10	+31	0.782***
	VPD _{y-1}	+99	+141	-0.639**		Tair	+10	+31	0.774***
	Tair _{y-1}	+78	+141	-0.627**		DL	+10	+38	0.765***
	REW _{y-1}	+134	+141	0.604**		VPD	+10	+31	0.712***
	Rg _{y-1}	+76	+118	-0.556**		REW	+9	+51	-0.709***
Short-scale	P_{y-1}	+77	+84	0.649**	P	+4	+46	-0.508*	
	P_{y-1}	+94	+115	0.638**	Tair	+10	+17	0.602**	
	P_{y-1}	+120	+134	0.623**	Short-scale (1 st part)	DL	+9	+16	0.583**
					VPD	+9	+16	0.559**	
					Rg	+9	+16	0.537*	
					DL	+18	+25	0.763***	
				Short-scale (2 nd part)	Rg	+15	+29	0.741***	
				Tair	+16	+30	0.652***		
				VPD	+20	+27	0.635**		

Table S2: Significant correlations extracted from the IPeak correlogram (Fig. S4). For a description of variables, window definitions and methodological notes, see Table S1.

<i>Current year</i>				
	Variable	Start	End	Correlation
Long-scale	Rg	+55	+125	0.673***
	Tair	+95	+200	0.668***
Short-scale (1 st part)	Rg	+70	+77	0.619**
	P	+70	+77	-0.584**
	VPD	+70	+77	0.45*
Short-scale (2 nd part)	VPD	+96	+103	0.789***
	Tair	+96	+103	0.712***
	Rg	+97	+104	0.593**
Short-scale (3 rd part)	Rg	+151	+158	0.743***
	VPD	+153	+181	0.595**
	Tair	+153	+202	0.58**
	P	+151	+158	-0.55**
	REW	+154	+161	-0.542**

Table S3: Significant correlations extracted from the IPeak correlogram excluding thinning and extreme summer years (Fig. S5). For a description of variables, window definitions and methodological notes, see Table S1.

<i>Previous year</i>					<i>Current year</i>				
	Variable	Start	End	Correlation		Variable	Start	End	Correlation
Long-scale	P_{y-1}	+57	+120	0.716**	Long- & short-scale	Tair	+22	+43	0.785**
Short-scale	P_{y-1}	+56	+63	0.828***		Rg	+12	+19	0.668*
	VPD _{y-1}	+56	+63	-0.636*		P	-33	+23	-0.64*
						VPD	+1	+43	0.574*

Table S4: Significant correlations extracted from the IDrop correlogram (Fig. S6), organized into two groups based on temporal proximity. For a description of variables, window definitions and methodological notes, see Table S1.

<i>Current year (1st group)</i>					<i>Current year (2nd group)</i>				
	Variable	Start	End	Correlation		Variable	Start	End	Correlation
Long-scale	Rg	+86	+128	0.769***	Long- & short-scale	REW	-70	-42	-0.83***
	Tair	+33	+131	0.899***		P	-67	-53	-0.538*
	VPD	+50	+162	0.932***		Rg	-66	-59	0.648**
	P	+31	+157	-0.725***					
	REW	+60	+207	-0.745***					
Short-scale (1 st part)	Tair	+39	+53	0.775***					
Short-scale (2 nd part)	Rg	+91	+112	0.748***					
	P	+92	+113	-0.549*					
Short-scale (3 rd part)	VPD	+107	+114	0.932***					
	Tair	+107	+114	0.856***					

Table S5: Significant correlations extracted from the IDrop correlogram excluding the 2003 drought year (Fig. S7), organized into two groups based on temporal proximity. For a description of variables, window definitions and methodological notes, see Table S1.

<i>Current year (1st group)</i>					<i>Current year (2nd group)</i>				
	Variable	Start	End	Correlation		Variable	Start	End	Correlation
Long-scale	Rg	+8	+113	0.789 ^{***}	Long- & short-scale	REW	-70	-42	REW
	Tair	+32	+137	0.834 ^{***}		P	-67	-53	P
	VPD	+53	+186	0.914 ^{***}		Rg	-66	-59	Rg
	P	+58	+142	-0.736 ^{***}					
	REW	+81	+207	-0.799 ^{***}					
	VPD	+92	+134	0.911 ^{***}					
	VPD	+71	+78	0.685 ^{***}					
Short-scale (1 st part)	Rg	+70	+77	0.594 ^{**}					
	P	+70	+84	-0.57 ^{**}					
	Tair	+70	+77	0.507 [*]					
Short-scale (2 nd part)	Rg	+92	+106	0.827 ^{***}					
	VPD	+92	+106	0.779 ^{***}					
	P	+92	+113	-0.588 ^{**}					
	VPD	+107	+114	0.822 ^{***}					
	Tair	+107	+114	0.781 ^{***}					
Short-scale (3 rd part)	VPD	+121	+128	0.78 ^{***}					
	P	+119	+126	-0.627 ^{**}					
	Rg	+121	+128	0.564 ^{**}					
	Tair	+122	+129	0.484 [*]					
Short-scale (4 th part)	VPD	+144	+158	0.765 ^{***}					
	REW	+138	+145	-0.756 ^{***}					
	Rg	+143	+157	0.524 [*]					